

Enhancing Quantum Dot Solar Cells Stability with a Semiconducting Single-Walled Carbon Nanotubes Interlayer Below the Top Anode

Jorge Mario Salazar-Rios, Nataliia Sukharevska, Mark Jonathan Speirs, Stefan Jung, Dmitry Dirin, Ryan M. Dragoman, Sybille Allard, Maksym V. Kovalenko, Ullrich Scherf, and Maria Antonietta Loi*

Semiconducting single-walled carbon nanotubes (s-SWNTs) are used as a protective interlayer between the lead sulfide colloidal quantum dot (PbS CQD) active layer and the anode of the solar cells (SCs). The introduction of the carbon nanotubes leads to increased device stability, with 85% of the initial performance retained after 100 h exposure to simulated solar light in ambient condition. This is in sharp contrast with the behavior of the device without s-SWNTs, for which the photoconversion efficiency, the open circuit voltage, the short-circuit current, and the fill factor all experiencing a sharp decrease. Therefore, the inclusion of s-SWNT as interlayer in CQD SCs, give rise to SCs of identical efficiency (above 8.5%) and prevents their performance degradation.

Colloidal quantum dots (CQDs) have shown to be a promising material for the fabrication of solar cells (SCs) from solution, displaying a power conversion efficiency (PCE) exceeding 13%.^[1] Lead halide (PbX) and especially lead sulfide (PbS) are among the most studied materials for CQD SCs. Recently PCEs of 12% have been achieved by enhancing the photocarrier diffusion length and thus it has become possible to make the active layer much thicker than before.^[2] Besides the impressive efficiency reached in fewer than eight years from the first certification, the interest in lead sulfide colloidal quantum dot (PbS CQD) SCs is also determined by their stability in ambient conditions, which makes them superior to several other emerging materials.^[3,4]

One of the peculiarities of PbS CQDs is the tailorability of their electronic properties, obtained both tuning their size and exploiting the properties of the ligands on their surface. Not


only are the ligands fundamental for the passivation of surface traps^[5,6] but it has been recently demonstrated that they allow for tuning the energy levels of PbS CQDs,^[7–9] and for controlling doping concentrations.^[10–12]

The state-of-the-art architecture for PbS CQD SCs takes advantage of such electronic tunability and uses a junction between an n-type layer of PbS, treated with tetrabutylammonium iodide (TBAI), and a p-type layer of PbS, which is treated with ethanedithiol (EDT).^[13–15] The PbS-TBAI/PbS-EDT structure not only results in the highest PCE^[14] but it has also shown a stable performance over a

period of 110 days when stored in dark and air.^[16–18] However, there are only a few studies where PbS CQD SCs were tested in an environment closer to real working conditions.^[19] In a recent work, Konstantatos and co-workers showed CQD SCs with a PbS-TBAI/PbS-EDT active layer stable under illumination in nitrogen atmosphere, which, however, degraded fast under concurrent exposure to ambient conditions and illumination.^[20]

Semiconducting single-walled carbon nanotubes (s-SWNTs) are an appealing building block for the fabrication of SCs, due to their outstanding properties, which include high chemical stability and remarkable charge mobility along the tube axis.^[21] SWNTs have already been successfully incorporated in perovskite SCs to fulfill the double function of hole transporting layer and protecting layer to improve the stability of devices.^[22–24] This has been explained with the hydrophobicity

Dr. J. M. Salazar-Rios, N. Sukharevska, Dr. M. J. Speirs, Prof. M. A. Loi
C. Zernike Institute for Advanced Materials
University of Groningen Nijenborgh 4
Groningen 9747, AG, The Netherlands
E-mail: m.a.loi@rug.nl

 The ORCID identification number(s) for the author(s) of this article can be found under <https://doi.org/10.1002/admi.201801155>.

© 2018 The Authors. Published by WILEY-VCH Verlag GmbH & Co. KGaA, Weinheim. This is an open access article under the terms of the Creative Commons Attribution-NonCommercial-NoDerivs License, which permits use and distribution in any medium, provided the original work is properly cited, the use is non-commercial and no modifications or adaptations are made.

DOI: 10.1002/admi.201801155

Dr. S. Jung, Dr. S. Allard, Prof. U. Scherf
Macromolecular Chemistry and Institute for Polymer Technology
Wuppertal University
Gauss-Str. 20, D-42119 Wuppertal, Germany

Dr. D. Dirin, R. M. Dragoman, Prof. M. V. Kovalenko
Institute of Inorganic Chemistry
Department of Chemistry and Applied Bioscience
ETH Zürich
Vladimir Prelog Weg 1, CH-8093 Zürich, Switzerland

Dr. D. Dirin, Prof. M. V. Kovalenko
Laboratory for Thin Films and Photovoltaics
Empa–Swiss Federal Laboratories for Materials Science and Technology
Überlandstrasse 129, CH-8600 Dübendorf, Switzerland

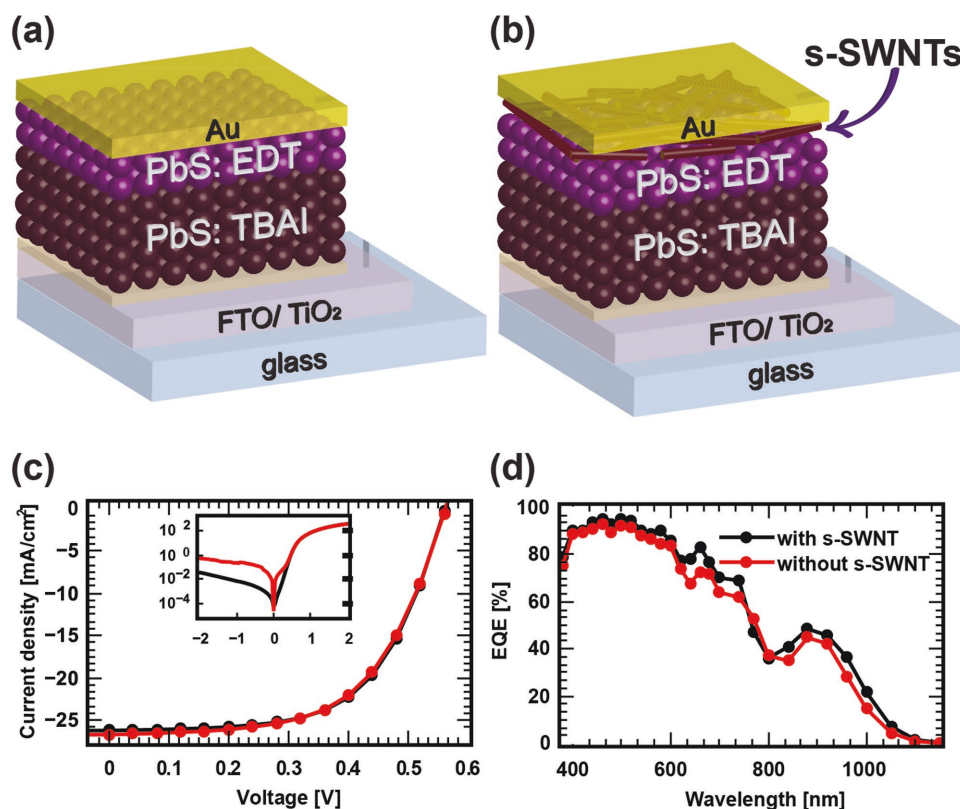


Figure 1. Device structure of the a) PbS CQD reference SC and of the b) PbS CQD SC with s-SWNT interlayer. c) J - V characteristics of SC devices with (black curve) and without (red curve) s-SWNTs-based interlayer under simulated AM1.5G solar illumination. The inset shows J - V measurements of the same devices in the dark. d) EQE spectra of the two types of devices.

of these nanocarbon materials which result in the protection of the active layer from the atmospheric humidity, which is highly harmful for hybrid perovskites.^[24]

Up until now, there are no data in the literature on the compatibility of CQD SCs with SWNTs. However, the use of conductive carbon paste as anode instead of gold has been reported to enhance the device stability.^[4]

Here we report the performance of PbS CQD SCs using s-SWNTs as an interlayer below the Au top anode. The PCE ($8.1\% \pm 0.6\%$) remained unaffected as compared to the devices without interlayer. The performance of both device types stored in dark and ambient condition was constant during the 78 days of testing. Importantly, under more demanding conditions, such as solar illumination in ambient condition, the SCs with the s-SWNT interlayer are profoundly more stable, with minimal performance reduction (15%) after more than 100 h of testing. This is in sharp contrast with the behavior of the device without SWNTs, which degraded to 20% of the initial efficiency during the same time.

The device structures of the fabricated SCs are depicted in **Figure 1a,b**. The PbS CQDs SCs are prepared as reported previously by several groups.^[14,25] A compact film of titanium oxide (TiO_2) is deposited as electron transporting layer on top of a pre-patterned fluorine-doped tin oxide layer on a glass substrate. The PbS CQD active layer is fabricated via layer-by-layer spin casting and is composed of two regions. In the first one, which is in contact with the TiO_2 layer, PbS CQDs

are treated with TBAI and the charge carrier transport is n-type dominated.^[7,26,27] The second region is treated with EDT, which results in a larger p-type character.^[7,28] The device structure is finished with the evaporation of the Au anode.

PbS CQDs SCs with this structure display PCEs above 8.5%.^[13,14,25,29] It has been proposed that the PbS-EDT layer acts as an electron-blocking/hole-extraction layer between the PbS-TBAI layer and the anode.^[14] Moreover, the different doping of the TBAI and the EDT layers controls the depletion width, which improves the charge carrier dissociation and allows for the implementation of thicker active layers that absorb more light.^[15] The insufficient hole concentration in the EDT-treated layer was in this context identified as a limiting factor in the device efficiency.^[15,25]

To obtain high-quality thin films of s-SWNT for the fabrication of the anode interlayer, we used the polymer wrapping technique to separate the semiconducting species from the metallic ones present in the initial SWNT sample. The s-SWNT ink was prepared using poly(3-dodecylthiophene-2,5-diyl) (P3DDT) to select HiPCO (high-pressure CO method) nanotubes following the procedure described in the supplementary information and reported earlier by Gomulya et al.^[30] The absorption spectra of the HiPCO:P3DDT ink is shown in Figure S1 in the Supporting Information. The sharp peaks in the infrared region represent the different chiralities of s-SWNTs present in the sample.^[30]

The resulting s-SWNT:polymer ink was used to prepare the device structure depicted in **Figure 1b**. The atomic force microscopy (AFM) measurements reported in **Figure S2**

Table 1. Summary of the figures of merit of the best SCs. These measurements were performed after 12 days when the SCs reached stable values.

Device	J_{SC} [mA cm^{-2}]	V_{OC} [V]	FF	PCE [%]
PbS SCs with s-SWNT	26.2	0.56	0.61	8.92
PbS SCs without s-SWNT	26.7	0.56	0.59	8.82

in the Supporting Information confirm the presence of the SWNTs on top of the active layer. Unfortunately, the s-SWNT network density cannot be determined from these measurements, as the CQD active layer has a larger roughness than the average diameter of the carbon nanotubes (≈ 1 nm).

The J - V characteristics of the best SCs with and without the s-SWNT under simulated AM1.5G solar illumination are reported in Figure 1c. The two device types exhibit similar performances with minor differences only in the J_{SC} and in the fill factor. This is an indication of the fact that the s-SWNT layer is thin enough to act exclusively as a tunneling barrier for the photogenerated carriers. The figures of merit of the two types of devices are reported in Table 1.

The external quantum efficiency (EQE) spectra of the two devices are reported in Figure 1d; also in this case the spectra are practically identical. We estimated that the thickness of the SWNTs interlayer is lower than 10 nm. Therefore, the light absorbed by the interlayer is negligible and its influence on the EQE is not detectable.

As mentioned above, another important characteristic SCs should have, besides efficiency, is stability under working conditions. We thus first examined the long-term stability of the two types of SCs when stored under ambient conditions in the dark. Figure 2 reports the figures of merit of the two devices measured in a nitrogen-filled glove box for 78 days.

After each measurement, the devices were stored back outside the glove box. The PCE of both devices increased within the first 12 days, from around 7% to almost 9%. This is mainly due to the increase in FF and V_{OC} and can be attributed to a further p-doping of the EDT-capped layer under influence of ambient oxygen. After 12 days, both devices reach a stable PCE, J_{SC} , and V_{OC} . These results are consistent with previous reports where similar devices were studied.^[14]

However, more realistic device stability tests involve constant exposure to solar light. We therefore studied the performance of our devices when exposed to concentrated illumination of 7 times AM1.5G in nitrogen atmosphere. Figure 3 reports the J - V characteristics of the devices at time zero (initial conditions), after 20 h of continuous illumination, and after the devices had been stored in the dark for 4 days. During the prolonged illumination, the SCs reached ≈ 340 K, which is ≈ 40 K higher than in standard testing conditions.

Both devices show a strong degradation of the main device parameters, namely V_{OC} and J_{SC} after 20 h of illumination. Therefore, when tested in nitrogen atmosphere, the s-SWNT interlayer does not appear to have any beneficial effect on the SCs. Interestingly, the degradation is partially reversible, and the SCs recover a large portion of their initial performance after few days of storage in the dark. The figures of merit of the devices after this test are summarized in Table 2.

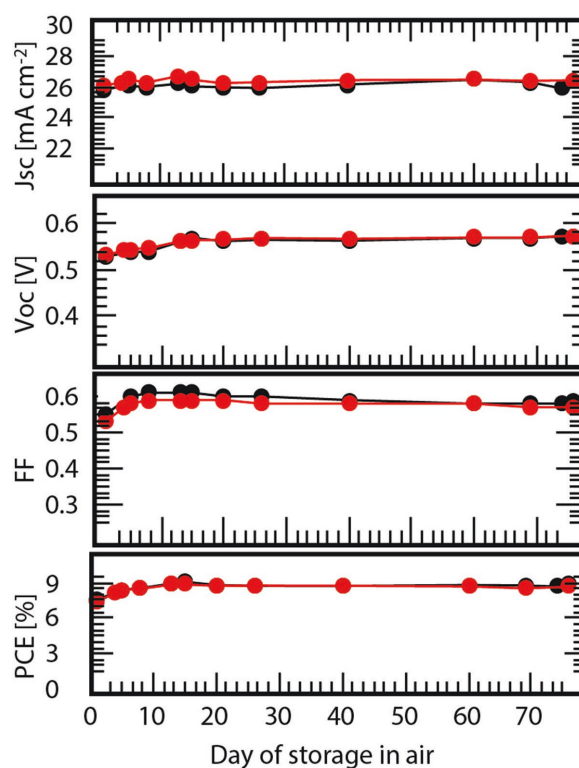


Figure 2. Device parameters over time of SCs with s-SWNT interlayer (black curve) and without interlayer (red curve). Both devices were stored in ambient conditions in the dark over a period of 78 days, and taken for measurements in a nitrogen-filled glove box.

At this point, it is important to investigate how our SCs behave at AM1.5G constant illumination in ambient conditions. Figure 4a reports the J - V characteristics of the two SC types continuously illuminated with AM1.5G for 105 h. The electrical parameters are shown in Figure 4b.

The SCs without the s-SWNT interlayer show a continuous degradation over a period of 105 h, with J - V characteristics gradually developing an s-shape. A closer look at the figures of merit shows that the J_{SC} and the FF decrease immediately after the beginning of the illumination, while the V_{OC} remains constant for the first 60 h. The rapid degradation of the V_{OC} results after 105 h in only the 50% of the initial value. The overall corruption of the figures of merit results in the decrease of the PCE of more than 75% in 105 h. This degradation, as shown in Figure S3 in the Supporting Information, is not reversible through storage in dark and N_2 atmosphere. We speculate that this is due to the chemical reaction of the active layer with oxygen and/or water. Degradation of PbS CQD SCs after illumination in air has also been observed previously, where the degradation was explained with the oxidation of the active material, which also drastically reduced the PCE of SCs that were stable in N_2 atmosphere.^[20]

Interestingly, the PbS CQD SCs with the s-SWNT interlayer show much better performance under prolonged illumination. The J - V characteristics remain more stable, and the figures of merit decrease only marginally. After 105 h of illumination, the PCE decreases only by 15%. These results demonstrate that the presence of the s-SWNT interlayer stabilizes PbS CQD SCs.

Table 2. Summary of the figures of merit of the SCs tested in different consecutive conditions, pristine, after 20 h illumination with 7 times AM1.5G illumination at 340 K, and after storage for 4 days in the dark.

Device		J_{sc} [mA cm ⁻²]	V_{oc} [V]	FF	PCE [%]
DPbS SCs with s-SWNT	(1) initial conditions	26.3	0.58	0.59	8.83
	(2) after 20 h illumination	23.8	0.51	0.47	5.74
	(3) after 4 days in the dark	26.2	0.54	0.54	7.67
PbS SCs without s-SWNT	(1) initial conditions	26.4	0.57	0.57	8.64
	(2) after 20 h illumination	23.6	0.51	0.45	5.36
	(3) after 4 days in the dark	25.8	0.53	0.53	7.16

We speculate, that the increased stability might be caused by the hydrophobicity of the carbon nanotube layer that prevents the interaction of water with the active layer.^[31] Another possibility is that the presence of the chemically stable s-SWNT interlayer avoids the interaction of photogenerated electrons with molecular oxygen, interaction that can trigger chemical reactions, which can be harmful for the stability of the active material.^[32] Here it is important to add that organic interlayers, as polythiophene derivatives such as P3DDT, do decrease the

performance of the device and are not able to protect the CQD active layer from ambient gasses. Therefore, this is a unique property demonstrated by the thin network of s-SWNTs.

In conclusion, we have demonstrated that PbS QD SCs including a thin layer of s-SWNT wrapped by P3DDT can withstand harsher stability tests under constant solar illumination in ambient condition for more than 100 h losing only 15% of their initial PCE. The SWNTs interlayer has an impressive role in protecting the active layer, which

without them degrades after 100 h of illumination losing ≈80% of the starting PCE.

Experimental Section

PbS CQD Synthesis: PbS CQDs capped with oleate ligands were synthesized by the hot injection method.^[33] As a Lead precursor, 1.516 g of Lead(II) acetate trihydrate (PbAc2·3H₂O) were used. PbAc2·3H₂O powder was dissolved in the mixture of 50 mL Octadecene (ODE) and 4.5 mL Oleic acid (OA). Then the Lead precursor solution was dried for 2 h under vacuum at 120 °C in a three-neck reaction flask, using a Schlenk line. As a Sulfur precursor, Bis(trimethylsilyl)sulfide (TMS₂S) was used, 0.420 mL of TMS₂S were dissolved in 10 mL of ODE in the nitrogen-filled glove box. The reaction was carried out under nitrogen atmosphere. The lead precursor solution was heated to 145 °C, and when the temperature reached this point, the sulfur precursor solution was quickly injected to the lead precursor solution. In the end, the heating mantle was removed, and the reaction was quenched by cooling the reaction flask down to room temperature using a cold-water bath. To isolate the nanocrystals, hexane and ethanol were added, followed by centrifugation. CQD was re-dispersed in hexane and precipitated with ethanol two more times (all of the washing steps were carried out in air). Finally, PbS CQDs were re-dispersed in hexane. Solution concentrations were determined by absorption, as well as by drying and weighing a small portion of the PbS CQD solution. For device fabrication, solution of PbS QDs with a first excitonic peak at 851 nm were used. This corresponded to QDs of 1.46 eV bandgap of 2.72 nm size.

Polymer Synthesis: The homopolymer P3DDT was synthesized as described previously^[34] and the molecular weights were measured using gel permeation chromatography. P3DDT was obtained after Soxhlet extraction with methanol, acetone, ethyl acetate, and hexane. For the experiments reported here, the hexane fraction with $M_n = 19.200$ g mol⁻¹ and $M_w = 22.300$ g mol⁻¹ was used.

Preparation and Characterization of Semiconducting SWNT Dispersion: HiPCO SWNTs (diameters between 0.8 and 1.2 nm) were purchased from Unidym Inc. The polymer was solubilized in toluene using a high power ultrasonicator (Misonix 3000) with cup horn bath (output power 69 W) for 10 min, followed by overnight stirring at 60 °C. Subsequently, SWNTs were added to form the SWNT:polymer dispersions with a weight ratio of 1:2 (3 mg of SWNTs, 6 mg of polymer, 15 mL of toluene). These solutions were then sonicated for 2 h at 69 W and 16 °C.

After ultrasonication, the dispersions were centrifuged at 30 000 rpm (109 000 g) for 1 h in an ultracentrifuge (Beckman Coulter Optima XE-90; rotor: SW55Ti) to remove all the remaining bundles and heavyweight impurities. After the centrifugation, the highest density components precipitate at the bottom of the centrifugation tube, while the low-density components, including small bundles and individualized SWNTs wrapped by the polymer, and free polymer chains, remain in the upper part (the supernatant).

One extra step of ultracentrifugation was implemented to decrease the amount of free polymer in solution (enrichment). For this purpose,

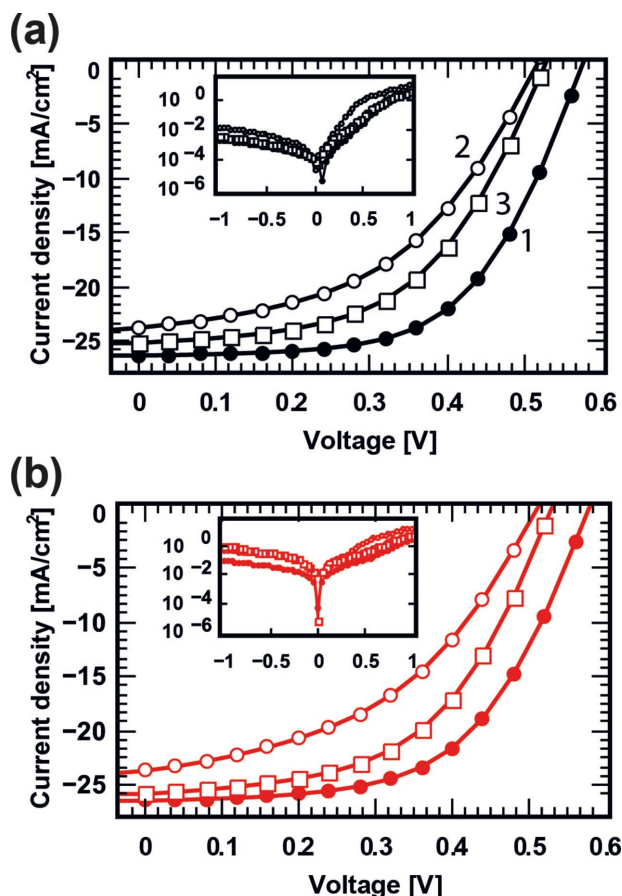


Figure 3. J - V characteristics of the PbS CQD SCs a) with and b) without s-SWNTs interlayer. The devices were measured at three points in time: 1) initial J - V curves (full circles), 2) after 20 h of illumination (7 times AM1.5) (empty circles), 3) after 20 h of illumination plus 4 days of storage in dark (empty squares). The two insets show the dark J - V characteristics.

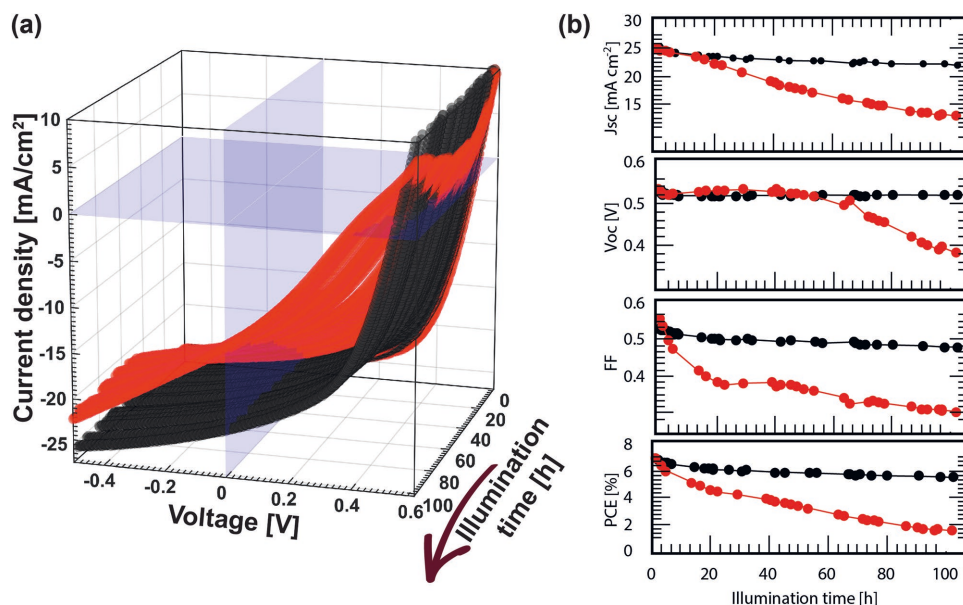


Figure 4. Stability of the J - V characteristics of PbS QCD SCs with (black curves) and without (red curves) s-SWNTs interlayer tested for 105 h under AM1.5G illumination in ambient conditions a) J - V curves at different times. b) Figures of merit (PCE, FF, V_{oc} , and J_{sc}) of the two devices at different testing times.

the supernatant obtained after the first ultracentrifugation was centrifuged for 5 h at 55 000 rpm (367 000 g), where the individualized s-SWNTs precipitated to form a pellet, and the free polymer remained in the supernatant. Finally, the pellet is re-dispersed by sonication in the solvent of choice.

Optical Characterization of the Semiconducting SWNT Dispersion: Optical measurements were performed to check the concentration of the carbon nanotubes selected by the polymer. Absorption spectra were recorded by a UV-Vis-NIR spectrophotometer (Shimadzu UV-3600).

Device Fabrication: Pre-patterned Fluorine-doped Tin oxide $\text{SnO}_2:\text{F}$ (FTO) glass substrates ($13 \Omega \text{ sq}^{-1}$), purchased from Visiontek Systems Ltd., were cleaned with detergent and then subsequently sonicated in acetone and isopropanol, and dried in an oven at 120°C for at least 20 min. Then, the FTO substrates were treated with O_3 to remove any possible organic residues and to improve wettability of the substrates. TiO_2 sol was prepared by mixing ethanol, titanium(IV) butoxide, and HCl (37%) in the ratio 20:2:1, then the sol was spin cast onto FTO substrates and annealed at 450°C for 30 min.

PbS QCDs films were deposited in a nitrogen-filled glove box. For the preparation of PbS QCDs films, the layer-by-layer spin casting method was used. PbS QCDs capped by Oleate ligands were spin cast from hexane solutions (10 mg mL^{-1}) onto the earlier prepared TiO_2 films. Ligand exchange was performed by exposing the films to the 15 mg mL^{-1} methanol solution of TBAI or acetonitrile solution of EDT, prepared in concentration of 0.01% by volume. Spin-drying removed the residuals of the ligands solutions. In order to get rid of the products of ligand exchange and the excess of unreacted ligands, films were washed twice with methanol or once with acetonitrile for the TBAI- and EDT-treated films, respectively. Cycles of deposition of the PbS QDs, ligand exchange, and washing were repeated 12 times for the TBAI-treated layers and 4 times for EDT-treated layers in order to reach the total thickness of 260 nm. PbS QCDs films were subjected to ambient conditions for 20 min to make the EDT layer more p-type.

The polymer-wrapped carbon nanotubes were spin casted on top of the PbS QCD film after air exposure. The s-SWNT dispersion was sonicated before deposition.

The devices were finalized by thermal evaporation of 80 nm gold under a pressure of 5×10^{-8} mBar with a rate of $0.5\text{--}2 \text{ \AA s}^{-1}$. The area of the SCs defined by the overlap of the FTO and Au electrodes is 0.16 cm^2 .

After Au deposition J - V characteristics of the devices were measured for the first time and after that, the devices were kept in air in the dark.

The average efficiency and standard deviation of the SCs was calculated from eight devices of each type.

Current-Voltage Characterization: J - V characteristics were measured in a nitrogen-filled glove box under simulated AM1.5G solar illumination, using a Steuernagel Solar constant 1200 metal halide lamp set to 100 mW cm^{-2} intensity and a Keithley 2400 source-meter. Light intensity was calibrated using a monocrystalline silicon solar cell (WRVS reference cell, Fraunhofer ISE) and corrected for the spectral mismatch. For PCE calculations, the illuminated area was confined by the shadow mask (0.10 cm^2) to avoid edge effects. The temperature was set to 295 K and controlled by a nitrogen gas flow through a liquid nitrogen bath.

For the stability test performed in air, J - V characteristics were measured under AM1.5G solar illumination with a solar simulator (SF150 class A, Sciencetech). The light intensity was adjusted in a way to get the same initial values of J_{sc} , as obtained using 100 mW cm^{-2} AM1.5 G solar light in nitrogen.

The EQE was measured under monochromatic light under short-circuit conditions. For the source of white light, a 250 W quartz tungsten halogen lamp (6334NS, Newport) with lamp housing (67009, Newport) was used. Narrow bandpass filters (Thorlabs) with a full width half maximum (FWHM) of $10 \pm 2 \text{ nm}$ from 400 to 1300 nm and a FWHM of $12 \pm 2.4 \text{ nm}$ from 1300 to 1400 nm are used. The light intensity is determined by calibrated PD300 and PD300IR photodiodes (Ophir Optics) for visible and infrared regions of the spectrum, respectively.

Morphology and Thickness Characterization: AFM measurements were obtained under ambient conditions with a Bruker microscope (MultiMode 8 with ScanAsyst) in ScanAsyst Peak Force Tapping mode with SCANASYST-AIR probes having elastic constant $k = 0.4 \text{ N m}^{-1}$, resonance frequency of 70 kHz, and tip radius lower than 12 nm (nominal 2 nm).

The images were taken with a scan rate of 0.98 Hz and the resolution of 1024 lines per sample. Thicknesses of the PbS QCDs films were measured by profilometer (Dektak 6M Stylus Profiler Veeco).

Supporting Information

Supporting Information is available from the Wiley Online Library or from the author.

Acknowledgements

J.M.S.-R. and N.S. contributed equally to this work. This work was part of the research programme of the Foundation for Fundamental Research on Matter (FOM), which is part of the Netherlands Organization for Scientific Research (NWO). This was a publication of the FOM-focus Group "Next Generation Organic Photovoltaics" participating in the Dutch Institute for Fundamental Energy Research (DIFFER). M.A.L. is grateful for the financial support of the European Research Council (ERC Starting Grant "Hy-SPOD" No. 306983). The authors are thankful to A. Kamp and T. Zaharia for technical support.

Conflict of Interest

The authors declare no conflict of interest.

Keywords

interlayer, quantum dots, single-walled carbon nanotubes, solar cells

Received: July 27, 2018

Revised: August 20, 2018

Published online: October 1, 2018

- [1] M. A. Green, Y. Hishikawa, E. D. Dunlop, D. H. Levi, J. Hohl-Ebinger, A. W. Y. Ho-Baillie, *Prog. Photovoltaics* **2018**, 26, 3.
- [2] J. Xu, O. Voznyy, M. Liu, A. R. Kirmani, G. Walters, R. Munir, M. Abdelsamie, A. H. Proppe, A. Sarkar, F. P. G. de Arquer, M. Wei, B. Sun, M. Liu, O. Ouellette, R. Quintero-Bermudez, J. Li, J. Fan, L. Quan, P. Todorovic, H. Tan, S. Hoogland, S. O. Kelley, M. Stefik, A. Amassian, E. H. Sargent, *Nat. Nanotechnol.* **2018**, 13, 456.
- [3] M. V. Kovalenko, *Nat. Nanotechnol.* **2015**, 10, 284.
- [4] J. An, X. Yang, W. Wang, J. Li, H. Wang, Z. Yu, C. Gong, X. Wang, L. Sun, *Sol. Energy* **2017**, 158, 28.
- [5] S. Kahmann, M. Sytnyk, N. Schrenker, G. J. Matt, E. Spiecker, W. Heiss, C. J. Brabec, M. A. Loi, *Adv. Electron. Mater.* **2018**, 4, 1700348.
- [6] A. H. Ip, S. M. Thon, S. Hoogland, O. Voznyy, D. Zhitomirsky, R. Debnath, L. Levina, L. R. Rollny, G. H. Carey, A. Fischer, K. W. Kemp, I. J. Kramer, Z. Ning, A. J. Labelle, K. W. Chou, A. Amassian, E. H. Sargent, *Nat. Nanotechnol.* **2012**, 7, 577.
- [7] P. R. Brown, D. Kim, R. R. Lunt, N. Zhao, M. G. Bawendi, J. C. Grossman, V. Bulovi, *ACS Nano* **2014**, 8, 5863.
- [8] R. W. Crisp, D. M. Kroupa, A. R. Marshall, E. M. Miller, J. Zhang, M. C. Beard, J. M. Luther, *Sci. Rep.* **2015**, 5, 9945.
- [9] D. M. Kroupa, M. Vörös, N. P. Brawand, B. W. McNichols, E. M. Miller, J. Gu, A. J. Nozik, A. Sellinger, G. Galli, M. C. Beard, *Nat. Commun.* **2017**, 8, 15257.
- [10] D. M. Balazs, K. I. Bijlsma, H.-H. Fang, D. N. Dirin, M. Döbeli, M. V. Kovalenko, M. A. Loi, *Sci. Adv.* **2017**, 3, 1558.
- [11] Q. Lin, H. J. Yun, W. Liu, H.-J. Song, N. S. Makarov, O. Isaienko, T. Nakotte, G. Chen, H. Luo, V. I. Klimov, J. M. Pietryga, *J. Am. Chem. Soc.* **2017**, 139, 6644.
- [12] A. R. Kirmani, A. Kiani, M. M. Said, O. Voznyy, N. Wehbe, G. Walters, S. Barlow, E. H. Sargent, S. R. Marder, A. Amassian, *ACS Energy Lett.* **2016**, 1, 922.
- [13] X. Lan, O. Voznyy, F. P. García de Arquer, M. Liu, J. Xu, A. H. Proppe, G. Walters, F. Fan, H. Tan, M. Liu, Z. Yang, S. Hoogland, E. H. Sargent, *Nano Lett.* **2016**, 16, 4630.
- [14] C.-H. M. Chuang, P. R. Brown, V. Bulovi, M. G. Bawendi, *Nat. Mater.* **2014**, 13, 796.
- [15] M. J. Speirs, D. N. Dirin, M. Abdu-Aguye, D. M. Balazs, M. V. Kovalenko, M. Antonietta Loi, *Energy Environ. Sci.* **2016**, 9, 2916.
- [16] S. Kim, A. R. Marshall, D. M. Kroupa, E. M. Miller, J. M. Luther, S. Jeong, M. C. Beard, *ACS Nano* **2015**, 9, 8157.
- [17] X. Yao, Z. Song, L. Mi, G. Li, X. Wang, X. Wang, Y. Jiang, *Sol. Energy Mater. Sol. Cells* **2017**, 164, 122.
- [18] S. Pradhan, A. Stavrinadis, S. Gupta, G. Konstantatos, *ACS Appl. Mater. Interfaces* **2017**, 9, 27390.
- [19] J. M. Luther, J. Gao, M. T. Lloyd, O. E. Semonin, M. C. Beard, A. J. Nozik, *Adv. Mater.* **2010**, 22, 3704.
- [20] Y. Cao, A. Stavrinadis, T. Lasanta, D. So, G. Konstantatos, *Nat. Energy* **2016**, 1, 16035.
- [21] R. Saito, G. Dresselhaus, M. S. Dresselhaus, *Physical Properties of Carbon Nanotubes*, Imperial College Press, London **1998**.
- [22] S. N. Habisreutinger, T. Leijtens, G. E. Eperon, S. D. Stranks, R. J. Nicholas, H. J. Snaith, *J. Phys. Chem. Lett.* **2014**, 5, 4207.
- [23] K. Aitola, K. Domanski, J.-P. Correa-Baena, K. Sveinbjörnsson, M. Saliba, A. Abate, M. Grätzel, E. Kauppinen, E. M. J. Johansson, W. Tress, A. Hagfeldt, G. Boschloo, *Adv. Mater.* **2017**, 29, 1606398.
- [24] S. N. Habisreutinger, R. J. Nicholas, H. J. Snaith, *Adv. Energy Mater.* **2017**, 7, 1601839.
- [25] M. J. Speirs, D. M. Balazs, D. N. Dirin, M. V. Kovalenko, M. A. Loi, *Appl. Phys. Lett.* **2017**, 110, 103904.
- [26] Z. Ning, H. Dong, Q. Zhang, O. Voznyy, E. H. Sargent, *ACS Nano* **2014**, 8, 10321.
- [27] Z. Ning, O. Voznyy, J. Pan, S. Hoogland, V. Adinolfi, J. Xu, M. Li, A. R. Kirmani, J.-P. Sun, J. Minor, K. W. Kemp, H. Dong, L. Rollny, A. Labelle, G. Carey, B. Sutherland, I. Hill, A. Amassian, H. Liu, J. Tang, O. M. Bakr, E. H. Sargent, *Nat. Mater.* **2014**, 13, 822.
- [28] D. M. Balazs, M. I. Nugraha, S. Z. Bisri, M. Sytnyk, W. Heiss, M. A. Loi, *Appl. Phys. Lett.* **2014**, 104, 112104.
- [29] M. Liu, O. Voznyy, R. Sabatini, F. P. G. de Arquer, R. Munir, A. H. Balawi, X. Lan, F. Fan, G. Walters, A. R. Kirmani, S. Hoogland, F. Laquai, A. Amassian, E. H. Sargent, *Nat. Mater.* **2017**, 16, 258.
- [30] W. Gomulya, J. M. Salazar Rios, V. Derenskyi, S. Z. Bisri, S. Jung, M. Fritsch, S. Allard, U. Scherf, M. C. dos Santos, M. A. Loi, *Carbon* **2015**, 84, 66.
- [31] S. N. Habisreutinger, T. Leijtens, G. E. Eperon, S. D. Stranks, R. J. Nicholas, H. J. Snaith, *Nano Lett.* **2014**, 14, 5561.
- [32] D. Bryant, N. Aristidou, S. Pont, I. Sanchez-Molina, T. Chotchunangatchaval, S. Wheeler, J. R. Durrant, S. A. Haque, *Energy Environ. Sci.* **2016**, 9, 1655.
- [33] M. J. Speirs, D. M. Balazs, H.-H. Fang, L.-H. Lai, L. Protesescu, M. V. Kovalenko, M. A. Loi, *J. Mater. Chem. A* **2015**, 3, 1450.
- [34] R. S. Loewe, S. M. Khersonsky, R. D. McCullough, *Adv. Mater.* **1999**, 11, 250.